Published in final edited form as:
Neuroimage. 2012 February 15; 59(4): 4055–4063. doi:10.1016/j.neuroimage.2011.08.053.

White Matter Atlas Generation using HARDI based Automated Parcellation

Luke Bloy[a], **Madhura Ingalhalikar**[a], **Harini Eavani**[a,b], **Robert T. Schultz**[b], **Timothy P.L. Roberts**[c], and **Ragini Verma**[a]

[a]Section of Biomedical Image Analysis, Department of Radiology, University of Pennsylvania, Philadelphia, PA 19104

[b]Center for Autism Research, Children's Hospital of Philadelphia, Philadelphia, PA, 19104

[c]Lurie Family Foundations MEG Imaging Center, Department of Radiology, Children's Hospital of Philadelphia, Philadelphia, PA, 19104

Abstract

Most diffusion imaging studies have used subject registration to an atlas space for enhanced quantification of anatomy. However, standard diffusion tensor atlases lack information in regions of fiber crossing and are based on adult anatomy. The degree of error associated with applying these atlases to studies of children for example has not yet been estimated but may lead to suboptimal results. This paper describes a novel technique for generating population-specific high angular resolution diffusion imaging (HARDI)-based atlases consisting of labeled regions of homogenous white matter. Our approach uses a fiber orientation distribution (FOD) diffusion model and a data driven clustering algorithm. White matter regional labeling is achieved by our automated data driven clustering algorithm that has the potential to delineate white matter regions based on fiber complexity and orientation. The advantage of such an atlas is that it is study specific and more comprehensive in describing regions of white matter homogeneity as compared to standard anatomical atlases. We have applied this state of the art technique to a dataset consisting of adolescent and preadolescent children, creating one of the first examples of a HARDI-based atlas, thereby establishing the feasibility of the atlas creation framework. The white matter regions generated by our automated clustering algorithm have lower FOD variance than when compared to the regions created from a standard anatomical atlas.

Keywords

Diffusion; Atlas Generation; HARDI Template; White Matter Parcellation

1. Introduction

The use of brain atlases in neuroimaging studies allows researchers to register, identify and perform measurements on individual subjects within a common spatial coordinate system

Corresponding Author: Luke Bloy, Section of Biomedical Image Analysis, 3600 Market St, Suite 380, Philadelphia PA 19104., lbloy@seas.upenn.edu.

enabling large scale group studies with greater statistical power to elucidate smaller or more subtle anatomical differences that exist in specific diseases. Since the introduction of the Talairach (Talairach 1988) human cortical atlas, a number of MRI atlases have been introduced to assist with these measurement issues. T1-weighted MR atlases (Collins, Holmes et al. 1995; Mazziotta, Toga et al. 1995; Lancaster, Woldorff et al. 2000; Mazziotta, Toga et al. 2001; Lancaster, Tordesillas-Gutierrez et al. 2007; Ashburner 2009) from the Montreal Neurological Institute (MNI) and the International Consortium of Brain Mapping (ICBM) have been used extensively to illustrate differences in gray matter anatomy as well as to localize functional signals within these structures. While T1-weighted MRI provides detailed information concerning cortical anatomy it provides considerably less information concerning white matter anatomy (Toga, Thompson et al. 2006), thus these atlases have focused primarily on the identification of GM regions, possessing limited information concerning WM regions.

By providing an in-vivo WM contrast mechanism, built on the recognition of the imaging consequences of diffusion anisotropy (Moseley, Cohen et al. 1990), diffusion tensor imaging (DTI) (Basser, Mattiello et al. 1994) has reinvigorated the study of WM pathologies and more recently DTI based WM atlases (Wakana, Jiang et al. 2004; Mori, Oishi et al. 2008; Oishi, Faria et al. 2009) have been introduced to address the relative lack of information provided by the existing cortical atlases. While DTI is able to model WM regions possessing a single fiber population, it is ill suited to model areas of more complex WM, such as fiber crossing. This limitation makes delineating boundaries within these regions difficult and the labeling within them suspect. More complex high angular resolution diffusion imaging (HARDI) data models (Frank 2002; Tournier, Calamante et al. 2004; Tuch 2004; Anderson 2005; Descoteaux, Angelino et al. 2007) have been developed to improve modeling in areas of complex WM. These new models provide contrast in areas of fiber crossing and orientation change that is unavailable from conventional DTI and better reflects the underlying structure of the WM tissue. This paper presents a novel methodology for building WM atlases by utilizing the HARDI contrast to identify and automatically label regions of homogenous WM. The utilization of an automated data driven clustering algorithm for region labeling permits the generation of population/study specific atlases without the need for manual delineation of anatomical regions.

In general, the utility of atlases are two-fold. First, an atlas provides a template image, either a population average or a single subject image, to serve as a spatial normalization target and thus defines a common spatial coordinate system. Secondly, each atlas identifies regions consisting of voxels that meet some conceptual criterion of *sameness*. The majority of imaging atlases attempt to label regions based on named neuroanatomical constructs, such as the prefrontal cortex or the internal capsule. This requires a neuroanatomist/neuroradiologist to manually label the template image to identify each region and is inherently variable, as human neuroanatomical boundaries are quite variable. Recent work within the registration community (Zhang, Avants et al. 2007; Hecke, Sijbers et al. 2008; Hamm, Ye et al. 2010; Hecke, Leemans et al. 2011) suggest that choosing a registration template from the population under study improves the accuracy of spatial normalization. However the labor intensive labeling process makes the accurate transfer of atlas defined regions to a population specific atlas difficult, a particularly acute issue when the population has unique characteristics (such as being of a younger age than the anatomical atlas) or when the new imaging modalities, such as HARDI, are being used.

It is also important to consider if labeling based on anatomical boundaries provide sufficient demarcation, particularly in areas of complex WM, for applications such as region of interest (ROI) based WM analysis. For instance, most large anatomical fiber bundles are known to traverse a variety of WM architectures and thus may not be well suited for region

of interest studies where they are represented by a single diffusion model or a single scalar feature, such as diffusion fractional anisotropy.

In this work we address these limitations of existing white matter atlases by presenting a framework to generate a population-specific HARDI atlas based on one of the prominent HARDI data models, the fiber orientation distribution (FOD) (Tournier, Calamante et al. 2004; Anderson 2005) function. The framework uses a non-linear spatial normalization algorithm to spatially transform the population into a common coordinate system and to create a population average FOD image. While we adopt a suitable registration algorithm, similar HARDI based registration techniques (Geng, Ross et al. 2011; Raffelt, Tournier et al. 2011; Yap, Chen et al. 2011) could be used in its place, without compromising the atlas framework and parcellation capability. The advantageous of algorithms of this type (i.e. based on HARDI) have been shown in registering areas of complex white matter when compared with state of the art DTI registration methods (Yap, Chen et al. 2011).

An automated data driven clustering routine is then applied to create a large number of spatial regions, each consisting of homogeneous WM architecture as measured by the FOD image. As regional homogeneity is the driving force behind the cluster process, each region is able to be confidently represented by its average, making these regions ideal for region of interest (ROI) statistical studies or for the extraction of spatial WM features for use in a classification framework. While neuroanatomical labeling may not provide suitable delineation of boundaries needed to identify homogeneous WM regions, it does aid in interpretability by providing researchers and clinicians with a means of investigating the structure/function of these regions as well as a comparative basis to other published studies. For this reason, in addition to determining homogeneous WM regions, we assign to each neuroanatomical labels based on its spatial overlap with an existing WM atlas. While not designed merely to identify these named anatomical constructs, the neuroanatomical relabeling of the data-based atlas, allows for describing the ROI as belonging to the anatomical region, thereby instilling it with joint information of the underlying fiber orientation as well as the global anatomy and function, facilitating interpretability.

We illustrate the application of our framework by generating a HARDI atlas from a dataset consisting of typically developing pediatric and young adolescent subjects, although the method is generalizable to any population under study. By comparing regional FOD spatial variances in anatomical labels to the variances computed from the regions determined by our clustering method, we demonstrate the ability our algorithms to generate atlases consisting of homogeneous WM regions well beyond what is achievable using the neuroanatomical labeling available in existing WM atlases. Average measures in these homogenous regions can then be used for subsequent statistical analysis and as the basis for between group and longitudinal within-group investigations. Anatomical interpretability of these study specific atlases generated by our method is imparted by establishing a correspondence with an existing atlas such as the EVE-DTI (Oishi, Faria et al. 2009) atlas in the presented case, but this could, in principle, be replaced by any anatomical atlas deemed of importance by the hypotheses of the study for which the atlas is being created.

2. Methods and Materials

This paper presents an automated method for creating a HARDI-based WM atlas for a given clinical population which will establish a common spatial reference frame to facilitate further investigation of WM differences. The generation of the WM atlas consists of a number of steps. First, an image of fiber orientation distribution (FOD) functions is computed for each subject's diffusion-weighted (DW)-MRI dataset. A non-linear spatial normalization process (Bloy and Verma 2010; Geng, Ross et al. 2011) is applied to deform

each subject's FOD image into the spatial domain defined by a single individual, chosen to act as the population template. Following registration, a population averaged FOD image is computed and a data driven clustering algorithm is applied (Bloy, Ingalhalikar et al. 2011) to divide the white matter into regions of homogenous WM architecture. This parcellation algorithm is designed to determine spatially compact regions that have a low spatial variance in the normalized FOD space and thus are comprised of voxels possessing both a similar orientation as well as a similar level of complexity (as imaging surrogates of low biological/tissue variance). These traits make these regions ideal candidates for regional statistical analysis (Kubicki, Westin et al. 2002; Alexander, Lee et al. 2007; Lee, Bigler et al. 2007; Fletcher, Whitaker et al. 2010) or as input features to a pattern classification method (Bloy, Ingalhalikar et al. 2011; Ingalhalikar, Parker et al. 2011). These regions are not necessarily intended to correspond directly to named anatomical structures provided by conventional labels such as the internal capsule, corpus callosum etc., but might for example expose sub-parcellation *within* such structures. To impart this additional anatomical information a labeling procedure is applied to assign WM labels derived from the EVE-DTI atlas ((Oishi, Faria et al. 2009) http://cmrm.med.jhmi.edu/cmrm/atlas/human_data/) to each region.

2.1. Fiber orientation distribution function

The fiber orientation distribution function (FOD) is the HARDI data model used in this work to quantify the WM architecture at each voxel. The FOD model (Tournier, Calamante et al. 2004; Anderson 2005) represents each voxel's DW-MRI signal as the spherical convolution of the FOD and the DW-MRI signal that would be measured for a single fiber bundle aligned along the z-axis. We utilized the constrained spherical deconvolution method (Tournier, Calamante et al. 2007) to compute the real spherical harmonic (RSH) representation of FOD, which is then normalized to have unit integral. Under this formulation the normalized FOD f is represented as $f(\theta,\varphi)=\sum_{l=0}\sum_{m=-l}^{l}\tilde{f}_{l,m}R_{l,m}(\theta,\varphi)$, where $R_{l,m}$ $(\theta\ \varphi)$ are the RSH basis functions and $\tilde{f}_{l,m}$ are the corresponding RSH coefficients. This representation allows for the efficient computation of the difference between two FODs using the L2 norm of the RSH coefficients as well as a means to rotate the FOD by the use of the Wigner D rotation matrices (Wigner 1931; Edmonds 1960). The FOD model is of particular interest in this work, as it contains information concerning both the orientation and partial volume fraction of any fiber bundles present within a voxel, making it well suited to model WM architecture in complex regions as well as those constituting a single fiber population.

2.2. Creating a population average FOD image

Once the FOD model has been fitted to each subject's DW-MRI dataset, a single subject is chosen to act as a template image for spatial normalization. Although any subject can be used to define the template spatial coordinate frame, it is generally best to choose the individual most representative of the population under study to act as the template subject. For instance, in generating the adolescent atlas in section 3, a twelve year old male subject served as the registration template.

With the template defined, the normalized FOD image of each subject is registered to the template FOD image via a two phase registration method (Figure 1), each phase utilizing a different similarity measure. The core of both registration phases is the multichannel diffeomorphic demons framework (Thirion 1998; Vercauteren, Pennec et al. 2009), discussed in the appendix A. The demons framework is designed to minimize an energy functional based on the difference metric between the fixed (template) and moving (subject) FOD images, F and M. By representing F and M in different feature spaces, the contribution

of orientation information to the demons algorithm can be managed in each registration phase, controlling the sensitivity of the registration method to the orientations of the FODs.

In the first phase, the demon's registration framework is used to minimize an orientation invariant metric between the FODs of the fixed and moving images (F and M), at each voxel, $\sqrt{\sqrt{\sum_{l=0,leven}^{lMax}(\sum_m(\tilde{f}_{l,m})^2 - \sum_m(\tilde{g}_{l,m})^2)}}$. As the basis functions of each RSH order (l level) span a subspace which is closed under rotations (Edmonds 1960; Frank 2002; Green 2003; Bloy and Verma 2010), the spectral power in the lth order, $\sum_{m=-1}^{l}(\tilde{f}_{l,m}(x))^2$ is a rotationally invariant feature of f. Therefore using the above metric in the spectral power space yields a registration process that is insensitive to rotations of the FODs of each image, allowing the computationally expensive reorientation process to be removed from this registration phase increasing its computational efficiency.

The second, orientation sensitive, registration phase uses the full vector of RSH coefficients to representation the FOD at each voxel, minimizing the L2 metric in the full RSH space, $\sqrt{\sqrt{\sum_{l=0,leven}^{lMax}\sum_m(\tilde{f}_{l,m} - \tilde{g}_{l,m})^2}} = \oint dw(f(\theta,\varphi) - g(\theta,\varphi))$. This metric measures the total amplitude difference between the two spherical functions, f and g, and is inherently sensitive to the orientations of both. Because of this sensitivity, during the demons optimization process, we reorient the moving image, using the finite strain reorientation scheme (Alexander, Pierpaoli et al. 2001), when applying the transformation at the current iteration. It may be noted that our registration algorithm can be replaced by similar HARDI based registration techniques (Geng, Ross et al. 2011; Raffelt, Tournier et al. 2011; Yap, Chen et al. 2011).

Following spatial normalization, each subject's FOD image has been registered into the same spatial coordinate system allowing the computation of the average FOD image for the population as well as the covariance matrix computation for the FOD coefficients. This average is obtained by averaging each RSH coefficient independently, which equates to the geometric mean performed in the RSH space. These mean and covariance images can serve both as a registration target for newly acquired subjects, as well as a simple first level analysis for identifying strong acute WM abnormalities such as lesions.

2.3. White Matter Parcellation

The process of parcellating the WM volume into spatially homogenous regions begins with the population average FOD image, as well as a binary image mask indicating which voxels consist of white matter tissue. Regions are then determined by using a spatially coherent normalized cuts algorithm (Bloy, Ingalhalikar et al. 2011) to cluster the WM volume. The algorithm, based on the superpixel (Mori 2005) methodology, works by iteratively dividing the most heterogeneous region into spatially connected parts until each of the resultant regions meet a homogeneity criterion. A region's heterogeneity ($\Phi(R)$) is represented by the average squared distance between the mean FOD (μ) and the FOD (f_i) of every voxel in the region.

$$\Phi(R) = \frac{1}{n}\sum_{i\in R}\left\|f_i - \mu\right\|_{L2}^2$$

This measure is related to the normalized trace of the FOD covariance matrix, and can therefore be interpreted similar to a variance.

The white matter volume is initially divided into a collection of regions, C, using a seed growing algorithm (appendix C) to identify any spatially disconnected components. From C we choose the region of the highest heterogeneity ($\Phi(R)$), which is then bipartitioned using the normalized cuts (N-Cut) algorithm, discussed in appendix B. The N-cut algorithm is mediated by the chosen form of the similarity function ($k(x_i,x_j)$). In this work we measure the similarity between two white matter voxels, with FODs and spatial locations given by f_i and p_i, using a product of a Gaussian kernel over the normalized FOD domain (standard deviation σ_f) and a Gaussian kernel (standard deviation σ_s) over the voxels' spatial locations.

$$k(x_i, x_j)=e^{-\frac{\left\|f_i-f_j\right\|_{L2}^2}{2\sigma_f}}\, e^{-\frac{\left\|p_i-p_j\right\|_{L2}^2}{2\sigma_s}}$$

The seed growing algorithm is then applied to each of the resultant regions, dividing any region that contains spatially disconnected components. Thus at each iteration, the region with the highest degree of non uniformity is replaced by spatially compact sub-regions. This process is repeated until every region has heterogeneity below a predefined threshold (ε). In order to control the generation of exceedingly small regions (< 5 voxels) that may be occasionally created, we apply a post processing step that identifies small regions and combines them with the neighboring region with the most similar mean FOD.

At the completion of automated clustering routine, the WM volume is divided into regions that have a degree of heterogeneity, as measured via the FODs, below the prescribed threshold. The boundaries of these regions are determined by the HARDI FOD contrast that is available within the data itself and thus takes full advantage of the contrast available from the HARDI.

2.4. Anatomical Labeling

It is advantageous, for instance when interpreting the location of abnormalities, to know the anatomical label of a specific region. This requires the additional step of labeling each of these data defined ROIs with anatomical labels provided by a co-registered anatomical atlas. We accomplish this by using an existing WM anatomical atlas, for instance the ICBM-DTI-81 (Mori, Oishi et al. 2008) or EVE-DTI atlases, to provide anatomical labels to each of the homogeneous WM regions that we determine. This is accomplished by using non-linear registration to spatially normalize the atlas' structural image to the population average structural image. The percent overlap between each WM region and the existing anatomical atlas regions are computed. For each WM region any anatomical label with greater than a 10% overlap is assigned to that WM region allowing for the possibility of multiple anatomical labels being assigned to regions that span the boundaries of anatomically defined regions.

The final result of the entire parcellation algorithm is a hierarchical two level white matter atlas. Each white matter voxel is first assigned a label representing which data driven ROI it belongs to. Secondly each of these ROIs is assigned a combination of anatomical labels based on the regional overlap to an existing anatomical atlas. The finer data driven ROIs are designed to consist of homogenous WM, as measured by a low FOD variance and may be useful for statistical analysis or to extract regional features to comprehensively represent a subject's WM architecture. The anatomical labels provide a more global anatomical context

to each ROI allowing both the location and in some cases function of each ROI to be ascertained and communicated to other researchers.

3. Results: Development of a population atlas (an illustrative example)

The problem of atlas generation or region of interest (ROI) delineation occurs in any population study where regional imaging measures serve for the basis of group comparison, such as ROI statistical analysis or subject based classification. The problem is however most acute when new imaging modalities, such as HARDI, are being utilized (for which no anatomical atlases exist) or when the population under study has not been used for generating atlases previously (such as in a younger population). For this reason, we illustrate the application of our WM atlas generation framework by creating a population atlas from a dataset of typically developing adolescent and preadolescent healthy subjects (6–18years). This specific population is of interest to many WM researchers involved in studies of younger populations at varying developmental stages, specifically those studying autism spectrum disorder and schizophrenia, which are believed to effect WM architecture and development (Kubicki, McCarley et al. 2007; Verhoeven, De Cock et al. 2010). This is an illustrative atlas, and may need to be regenerated with a larger sample size, or to suit specific clinical purposes.

3.1. Imaging dataset

The dataset consisted of 23 typically developing children (TDC) between the ages of 6 and 18 years (mean 11.2 ± 2.7 years). All participants were carefully screened, using parent report questionnaires and a telephone interview, to insure that they did not have a history of current or prior neuropsychiatric symptomatology. Moreover, T1 weighted brain images were evaluated clinically by a board certified neuroradiologist and all participants in this study were found to completely anomaly free. For each subject a whole brain HARDI dataset was acquired using a Siemens 3T Verio™ MRI scanner using a monopolar Stejskal-Tanner diffusion weighted spin-echo, echo-planar imaging sequence (TR/TE=14.7s/110ms, 2mm isotropic voxels, b=3000 s/mm^2, number of diffusion directions=64, 2 b0 images, scan time 18 minutes). In order to facilitate tissue segmentation as well the coregistration with an existing atlas lacking a HARDI component, such as the EVE-DTI or the ICBM-152, a structural image was acquired, using an MP-RAGE imaging sequence (TR/TE/TI = 19s/ 2.54ms/.9s, 0.8mm in plane resolution, 0.9mm slice thickness).

3.2. DW-MRI and Structural preprocessing

Prior to computing the FOD image from each subject's DW-MRI image a number of preprocessing steps were performed in order to reduce imaging artifacts and improve signal to noise. First, the DW-MRI images were filtered using a joint linear minimum mean squared error filter to remove Rician noise (Tristán-Vega and Aja-Fernández 2010). This was followed by eddy current and motion correction performed via the affine registration of each DW-MRI volume to the non diffusion-weighted (b0) image (Jezzard, Barnett et al. 1998). The normalized FOD image for each subject was then computed using the constrained spherical deconvolution method (Tournier, Calamante et al. 2007) and normalized to have unit integral.

Using each subject's structural MP-RAGE image, their white matter segmentation was determined by the following procedure. Skull-stripping and bias field correction were performed using the BET (Smith 2002) tool and N3 bias correction (Sled, Zijdenbos et al. 1998). Tissue segmentation was then performed, to identify cerebrospinal fluid, gray and white matter voxels, using an adaptive K-means clustering (Pham and Prince 1999). A rigid body registration, between the b0 image and the bias corrected structural image was

performed. Using this deformation field, the white matter segmentation mask was then resampled into the diffusion space yielding a white matter segmentation mask for each subject.

3.3. Registration

The FOD image of each subject was then non-linearly registered to that of a 12 year old male, who was chosen to serve as the template subject. An affine registration between the b0 images, was performed using the FLIRT (Jenkinson and Smith 2001) software tool. This transformation was then used to initialize the two phase registration method described in section 2.2. Once this process was completed for each of the 23 subjects, a population average FOD image was computed by averaging each RSH component of the registered subject FOD images individually. Using the computed deformation fields, each subject's WM segmentation mask was deformed into the template coordinate frame and then averaged and thresholded to yield a binary mask describing the voxels that were considered WM in over 40% of the subjects. These 2 images, the population average FOD image and the population WM mask are then used to determine the atlas regions.

The benefits of using nonlinear spatial registration to determine the population template image, as opposed to affine registration used in several of the existing population atlases (Mazziotta, Toga et al. 1995; Mori, Oishi et al. 2008), are illustrated through a marked decrease in the voxelwise FOD variance across the sample. The FOD variance at a voxel, x, is determined by $v(x)=\frac{1}{n}\sum_i \left\| f_i - \mu \right\|_{L2}^2$.

Variance maps computed following the affine registration (Panel A) and our registration method (Panel B) are shown in Figure 2. These results show a global decrease in the FOD variance while drastically reducing the variance in key central WM regions, indicating a clear benefit from using the non-linear registration algorithm.

3.4. Region Delineation

The key aspect of our atlas generation framework is the method described in section 2.3 used to delineate regions of spatially homogeneous WM. Our automated WM parcellation method was applied using the population average FOD image to model the WM architecture and using the population WM mask to identify WM voxels.

An investigation of the parameters used to define the WM similarity kernel, σ_f and σ_s, as well as the stopping variance threshold, ε, was performed. Adjusting the σ_f and σ_s parameters had the expected behavior of controlling the spatial smoothness of the determined regions. Similar results, in terms of both the number of regions, average region size, and average regional FOD variance were found when varying σ_f in the 0.1 – 0.3 range and σ_s in the 6mm – 10mm range. Adjusting ε has the most direct effect on the resulting parcellations as it determines at what point the subdivision process is halted. Figure 3 shows the results of our method as ε is changed between 0.06 and 0.1. As ε is decreased there is a clear decrease in the regional variance as well as an increase in the number of regions determined, resulting in a coarser regional delineation. This relationship, between the achieved regional variance and the number of regions, suggests that in practice this parameter must be tailored to the population under study as well as to the intended use of the derived atlas regions.

Based on these results, two atlases were generated. A coarse atlas was generated using the parameters σ_s = 6mm, σ_f = 0.3 and ε = 0.15 while the finer atlases used a lower halting threshold of ε = 0.08. The iterative nature of the parcellation algorithm yields a hierarchical

relationship between these atlases, with the ε = 0.15 regions being supersets of the ε = 0.08 regions. The finer atlas consists of 379 spatially compact regions with an average regional size of 105 2mm^3 voxels and a mean regional FOD variance of 0.06, while the coarse atlas consists of 94 regions with an average regional size of 423 2 mm^3 voxels and mean regional FOD variance of 0.10. Representative coronal slices of the coarse and fine atlases are shown in Figure 4. The rough bilateral symmetry of the regions is clearly visible in the coarse atlas, while at the finer scale the bilaterality is less apparent particularly in complex WM regions. Figure 5 shows representative slices of the finer atlas and corresponding regional FOD variance maps. The orientation sensitive aspect of the similarity kernel groups voxels with similar orientation, as seen in the genu and splenium of the corpus callosum, while sensitivity to the WM complexity aids in parcellating the cortical WM.

3.5. Comparison with anatomical atlas defined regions

We utilized the EVE-DTI atlas to create an anatomical WM parcellation that would be used both as a comparison as well as to provide our data defined regions with anatomical context as described in section 2.4. This was achieved by using a nonlinear spatial normalization algorithm to transform the structural, T1 weighted image provided as part of the EVE-DTI atlas into the space defined by the group average T1-weighed image (T1-weighted images were used for registration as this was the common modality between the HARDI population and the DTI anatomical atlas). Using this deformation field, the anatomical labels provided by the EVE-DTI atlas were then transformed into the template space yielding an alternative parcellation. Figure 6 shows a comparison between the population atlases, generated using ε = 0.15 and ε = 0.08, and the anatomical regions inherited from the EVE-DTI atlas. A clear improvement in regional FOD variance is achieved using the ε = 0.15 data driven atlas regions, with a further improvement at the expense of generating a moderately larger number of regions when using the finer atlas (ε = 0.08).

4. Discussion

We have proposed an automated atlas building method that utilizes HARDI data and the FOD diffusion model to provide improved contrast in complex WM regions using a non-linear spatial normalization to more accurately determine spatial correspondence and a novel data-driven WM parcellation algorithm that allows automated regional labeling based on models of the local WM architecture as opposed to the traditional time consuming anatomical labeling. The automatic nature of these methods permits researchers to generate their own atlas based on the datasets of their specific study. This overcomes many issues that occur when attempting to use published atlases, such as different clinical populations (ages) or imaging protocols being utilized to generate the atlas.

Similar to the cytoarchitectural mapping of the brain (Brodmann 1909), where local variations in cell type are used to delineate cortical regions, our method uses the FOD as a non-invasive imaging measure of local tissue architecture to delineate WM regions. Through the application of this methodology to the problem of generating an age specific population atlas, adolescent and preadolescent healthy subjects in our case, we show that these regions are more homogenous, with respect to WM orientation and complexity, than the regions inherited from an existing DTI based anatomical atlas. This suggests that these regions are better suited for regional statistical analysis or the extraction of regional features of WM architecture to be used in subsequent applications such as pattern classification and are thus perhaps more faithful to the overall goal of identifying regions of biological homogeneity.

The generation of the illustrative WM atlas shows that both the spatial normalization and WM parcellation methods outperform the typical processing methods that are generally utilized for determining WM atlases. A comparison of voxel wise population variance maps,

figure 2, generated from the non-linear and affine registration shows the clear improvement in both global and focal variances when using the non-linear registration technique. This decrease in FOD variance is critical for the accurate computation of the population average FOD image and the stability of the final atlas regions. Similarly, a comparison between the anatomical regions of the EVE-DTI atlas and those determined by our method, shown in figure 5, indicate the benefit of using data-driven regions to represent local WM architecture, through the marked decrease in regional FOD variance. This decrease suggests that the data determined regions are more tightly related to the local WM anatomy, which may have significant benefits when examining clinical populations (e.g., schizophrenia, autism spectrum disorder). While bilateral symmetry is not considered in the region delineation process, the roughly bilateral nature of WM anatomy is still clearly apparent in the data defined regions, shown in figure 4, particularly at the coarser spatial scalars.

The proposed framework provides three parameters which affect the regions that are determined. Of these three, the stopping criterion, ε, has the most pronounced affect, seen in figure 3, on both the number of regions determined and, more significantly, the regional FOD variances of these regions. The other 2 parameters, σ_s and σ_f, determine the kernels used in the similarity functions, affecting the smoothness of the ROIs, in the spatial and feature domain and in turn, the number and size of the resulting regions but had little effect on the regional FOD variance of the regions. In practice, selection of ε should be based on the desired degree of uniformity required for the regions while the other parameters are best set based on qualitative assessment of the resulting atlas. This process need only be done once for a new population and requires little effort particularly when compared with the process of manually correcting anatomical regions.

The stability of the clustering, in terms of specific boundary locations, is mainly governed by the robustness of the population average. For this reason it is important to ensure that a sufficient number of subjects are used to make up the population average. If this number is suitably large the effect of additional subjects on the population average and thus on the parcellation results will be negligible. In practice, the study specific atlas is generated when the study is ready for a statistical analysis. The atlas is created once, using the sample size determined by the study's power calculations, and reflects the local variation in the specific dataset.

While the focus of this work has been on the delineating homogenous WM regions, the ability to include global anatomical information into the regions is also important. This anatomical information not only improves the interpretation of any subsequent results by providing anatomical context to the regions, aiding in hypothesis formulation, but also facilitates meta-analytic studies by utilizing existing anatomical terminology. In our case we have used the EVE-DTI WM atlas to impart this global information; however, any anatomical atlas can, in principle, be used in the method. For instance, as developmental studies progress, the inclusion of pediatric anatomical and functional atlases can be incorporated for various ages. The ability to assign domain specific labels, either functional or otherwise, to the WM regions determined by our method yields a multi-faceted approach to atlas creation, giving researchers tremendous flexibility concerning the information content available in the atlas, which will prove extremely useful as research protocols move towards utilizing multiple modalities.

The fact that this paper describes an atlas generation methodology as opposed to simply the description of a single population HARDI atlas, like the ICBM-DTI-81 (Mori, Oishi et al. 2008), is indicative of our belief that optimal results from a group study are obtained when the specific traits of the population and data are utilized. While we have focused on WM, developing novel clustering methods based on the state of the art modeling of WM

architecture, the central theme of his work is applicable to many other atlas building problems. For instance gray matter regions could be parcellated based on their structural and functional connectivity profiles, ostensibly generating regions that more closely respect the structure/function relationship within the population understudy.

It is important to note that while the method presented in this paper makes use of high b-value (3000 s/mm^2) HARDI data, the principles of the clustering algorithm can be extended to other diffusion models and other b-values. A method that makes use of the diffusion tensor model acquired on lower b-value data is currently under development. While such a method will prove useful to many researchers, as DTI is now routinely acquired, it is still unclear how parcellations generated from DTI will compare with those generated using HARDI. It is similarly unclear exactly how large a role the improved angular resolving power garnered from high b-value HARDI data plays in the WM parcellation. Based on the improvements of modeling complex WM regions using HARDI data models at higher b-values one might expect better delineation in regions of fiber crossing etc. However the definitive comparison will have to wait until a technically-suitable dataset consisting of both HARDI and DTI data has been acquired on the same subjects.

In conclusion this paper presents a methodology for creating HARDI white matter atlases using the fiber orientation distribution (FOD) diffusion model. The automated nature of the methods allows for their efficient application to any population without relying on the time consuming task of manual anatomical delineation. The resulting atlas consists of regions designed to be homogenous with respect to the local architecture of the WM and are thus ideally suited for either statistical analysis or to be used as features within a pattern classification framework.

Acknowledgments

This research was supported by the NIH grants T32-EB000814(LB), R01-MH079938 (RV), R01-MH092862 (RV), R01-DC008871 (TR), a grant from the Nancy Lurie Marks Family Foundation (TR) and the Center grant SAP#4100047863 (RS). Dr Roberts would like to thank the Oberkircher Family for the Oberkircher Family Chair in Pediatric Radiology.

References

Alexander AL, Lee JE, et al. Diffusion tensor imaging of the corpus callosum in Autism. Neuroimage. 2007; 34(1):61–73. [PubMed: 17023185]

Alexander DC, Pierpaoli C, et al. Spatial transformations of diffusion tensor magnetic resonance images. Medical Imaging, IEEE Transactions on. 2001; 20(11):1131–1139.

Anderson AW. Measurement of fiber orientation distributions using high angular resolution diffusion imaging. Magnetic Resonance in Medicine. 2005; 54(5):1194–1206. [PubMed: 16161109]

Ashburner J. Computational anatomy with the SPM software. Magn Reson Imaging. 2009; 27(8): 1163–1174. [PubMed: 19249168]

Basser PJ, Mattiello J, et al. Estimation of the effective self-diffusion tensor from the NMR spin echo. J Magn Reson B. 1994; 103(3):247–254. [PubMed: 8019776]

Bloy L, Ingalhalikar M, et al. HARDI based Pattern Classifiers for the Identification of White Matter Pathologies. Med Image Comput Comput Assist Interv Int Conf Med Image Comput Comput Assist Interv. 2011

Bloy L, Ingalhalikar M, et al. Neuronal white matter parcellation using spatially coherent normalized cuts. Proc IEEE Int Biomedical Imaging: From Nano to Macro Symp. 2011

Bloy L, Verma R. Demons registration of high angular resolution diffusion images. Proc IEEE Int Biomedical Imaging: From Nano to Macro Symp. 2010

Brodmann, K. Vergleichende Lokalisationslehre der Grosshirnrinde in ihren Prinzipien dargestellt auf Grund des Zellenbaues. Leipzig: Johann Ambrosius Barth Verlag; 1909.

Collins DL, Holmes CJ, et al. Automatic 3-D model-based neuroanatomical segmentation. Human Brain Mapping. 1995; 3(3):190–208.

Descoteaux M, Angelino E, et al. Regularized, fast, and robust analytical Q-ball imaging. Magnetic Resonance in Medicine. 2007; 58(3):497–510. [PubMed: 17763358]

Edmonds, AR. Angular Momentum in Quantum Mechanics. Princeton University Press; 1960.

Fletcher PT, Whitaker RT, et al. Microstructural connectivity of the arcuate fasciculus in adolescents with high-functioning autism. Neuroimage. 2010; 51(3):1117–1125. [PubMed: 20132894]

Frank LR. Characterization of anisotropy in high angular resolution diffusion-weighted MRI. Magnetic Resonance in Medicine. 2002; 47(6):1083–1099. [PubMed: 12111955]

Geng X, Ross TJ, et al. Diffeomorphic image registration of diffusion MRI using spherical harmonics. IEEE Trans Med Imaging. 2011; 30(3):747–758. [PubMed: 21134814]

Green, R. Spherical Harmonic Lighting: The Gritty Details. Archives of the Game Developers Conference; 2003.

Hamm J, Ye DH, et al. GRAM: A framework for geodesic registration on anatomical manifolds. Med Image Anal. 2010; 14(5):633–642. [PubMed: 20580597]

Hecke WV, Leemans A, et al. The effect of template selection on diffusion tensor voxel-based analysis results. NeuroImage. 2011; 55(2):566–573. [PubMed: 21146617]

Hecke WV, Sijbers J, et al. On the construction of an inter-subject diffusion tensor magnetic resonance atlas of the healthy human brain. NeuroImage. 2008; 43(1):69–80. [PubMed: 18678261]

Hernandez V, Roman JE, et al. SLEPc: A Scalable and Flexible Toolkit for the Solution of Eigenvalue Problems. ACM Transactions on Mathematical Software. 2005; 31(3):351–362.

Ingalhalikar M, Parker D, et al. Diffusion based abnormality markers of pathology: Toward learned diagnostic prediction of ASD. NeuroImage. 2011

Jenkinson M, Smith S. A global optimisation method for robust affine registration of brain images. Med Image Anal. 2001; 5(2):143–156. [PubMed: 11516708]

Jezzard P, Barnett AS, et al. Characterization of and correction for eddy current artifacts in echo planar diffusion imaging. Magn Reson Med. 1998; 39(5):801–812. [PubMed: 9581612]

Kubicki M, McCarley R, et al. A review of diffusion tensor imaging studies in schizophrenia. J Psychiatr Res. 2007; 41(1–2):15–30. [PubMed: 16023676]

Kubicki M, Westin CF, et al. Uncinate fasciculus findings in schizophrenia: a magnetic resonance diffusion tensor imaging study. Am J Psychiatry. 2002; 159(5):813–820. [PubMed: 11986136]

Lancaster JL, Tordesillas-Gutierrez D, et al. Bias between MNI and Talairach coordinates analyzed using the ICBM-152 brain template. Hum Brain Mapp. 2007; 28(11):1194–1205. [PubMed: 17266101]

Lancaster JL, Woldorff MG, et al. Automated Talairach atlas labels for functional brain mapping. Hum Brain Mapp. 2000; 10(3):120–131. [PubMed: 10912591]

Lee JE, Bigler ED, et al. Diffusion tensor imaging of white matter in the superior temporal gyrus and temporal stem in autism. Neuroscience letters. 2007; 424(2):127–132. [PubMed: 17714869]

Mazziotta J, Toga A, et al. A probabilistic atlas and reference system for the human brain: International Consortium for Brain Mapping (ICBM). Philos Trans R Soc Lond B Biol Sci. 2001; 356(1412):1293–1322. [PubMed: 11545704]

Mazziotta JC, Toga AW, et al. A probabilistic atlas of the human brain: theory and rationale for its development. The International Consortium for Brain Mapping (ICBM). NeuroImage. 1995; 2(2): 89–101. [PubMed: 9343592]

Mori G. Guiding Model Search Using Segmentation. IEEE International Conference on Computer Vision. 2005; 2:1417–1423.

Mori S, Oishi K, et al. Stereotaxic white matter atlas based on diffusion tensor imaging in an ICBM template. Neuroimage. 2008; 40(2):570–582. [PubMed: 18255316]

Mori S, Oishi K, et al. Stereotaxic white matter atlas based on diffusion tensor imaging in an ICBM template. Neuroimage. 2008; 40(2):570–582. [PubMed: 18255316]

Moseley ME, Cohen Y, et al. Diffusion-weighted MR imaging of anisotropic water diffusion in cat central nervous system. Radiology. 1990; 176(2):439–445. [PubMed: 2367658]

Oishi K, Faria A, et al. Atlas-based whole brain white matter analysis using large deformation diffeomorphic metric mapping: application to normal elderly and Alzheimer's disease participants. NeuroImage. 2009; 46(2):486–499. [PubMed: 19385016]

Pham DL, Prince JL. Adaptive fuzzy segmentation of magnetic resonance images. IEEE Trans Med Imaging. 1999; 18(9):737–752. [PubMed: 10571379]

Raffelt D, Tournier JD, et al. Symmetric diffeomorphic registration of fibre orientation distributions. NeuroImage. 2011; 56(3):1171–1180. [PubMed: 21316463]

Rahimi A, Recht B. Clustering with Normalized Cuts is Clustering with a Hyperplane. Statistical Learning in Computer Vision. 2004

Shi JB, Malik J. Normalized cuts and image segmentation. Ieee Transactions on Pattern Analysis and Machine Intelligence. 2000; 22(8):888–905.

Sled JG, Zijdenbos AP, et al. A nonparametric method for automatic correction of intensity nonuniformity in MRI data. IEEE Trans Med Imaging. 1998; 17(1):87–97. [PubMed: 9617910]

Smith SM. Fast robust automated brain extraction. Hum Brain Mapp. 2002; 17(3):143–155. [PubMed: 12391568]

Talairach, J. Co-Planar Stereotaxic Atlas of the Human Brain: 3-D Proportional System: An Approach to Cerebral Imaging. New York: Thieme; 1988.

Thirion JP. Image matching as a diffusion process: an analogy with Maxwell's demons. Med Image Anal. 1998; 2(3):243–260. [PubMed: 9873902]

Toga AW, Thompson PM, et al. Towards multimodal atlases of the human brain. Nat Rev Neurosci. 2006; 7(12):952–966. [PubMed: 17115077]

Tournier JD, Calamante F, et al. Robust determination of the fibre orientation distribution in diffusion MRI: Non-negativity constrained super-resolved spherical deconvolution. NeuroImage. 2007; 35(4):1459–1472. [PubMed: 17379540]

Tournier JD, Calamante F, et al. Direct estimation of the fiber orientation density function from diffusion-weighted MRI data using spherical deconvolution. NeuroImage. 2004; 23(3):1176–1185. [PubMed: 15528117]

Tristán-Vega A, Aja-Fernández S. DWI filtering using joint information for DTI and HARDI. Med Image Anal. 2010; 14(2):205–218. [PubMed: 20005152]

Tuch DS. Q-ball imaging. Magnetic Resonance in Medicine. 2004; 52(6):1358–1372. [PubMed: 15562495]

Vercauteren T, Pennec X, et al. Diffeomorphic demons: efficient non-parametric image registration. Neuroimage. 2009; 45(1 Suppl):S61–S72. [PubMed: 19041946]

Verhoeven JS, De Cock P, et al. Neuroimaging of autism. Neuroradiology. 2010; 52(1):3–14. [PubMed: 20033797]

Wakana S, Jiang H, et al. Fiber Tract-based Atlas of Human White Matter Anatomy. Radiology. 2004; 230(1):77–87. [PubMed: 14645885]

Wigner, EP. Gruppentheorie und ihre Anwendungen auf die Quantenmechanik der Atomspektren. Vieweg Verlag; Braunschweig: 1931.

Yap PT, Chen Y, et al. SPHERE: SPherical Harmonic Elastic REgistration of HARDI data. NeuroImage. 2011; 55(2):545–556. [PubMed: 21147231]

Zhang H, Avants BB, et al. High-dimensional spatial normalization of diffusion tensor images improves the detection of white matter differences: an example study using amyotrophic lateral sclerosis. IEEE Trans Med Imaging. 2007; 26(11):1585–1597. [PubMed: 18041273]

Appendix A. Multichannel Diffeomorphic Demons

Given a fixed and moving image, F and M, the diffeomorphic demons algorithm seeks to determine a correction to the current transformation, s, of the form exp(u). This update minimizes a global energy functional, $E_s(u)=\sum_{p\in\Omega}\left\|F(p)-M\circ s\circ exp(u(p))\right\|_{L2}^2+\left(\frac{\sigma_i}{\sigma_x}\right)^2\left\|u\right\|^2$,

where p are points in Ω, the domain of the fixed image, F. The $\frac{\sigma_i}{\sigma_x}$ term accounts for image noise and interpolation error and acts as a regularizer for determining the update field. We can linearize the image similarity term in the region of u = 0 as $F(p) - M \circ s \circ exp(u(p)) = F(p) - M \circ s(p) + J_p u$ and in the case where F and M are images of vectors, J_p is the Jacobian matrix. With this linearization the energy functional simplifies to

$$E_s(u) = \sum_{p \in \Omega} \left\| \begin{bmatrix} F(p) - M^{\circ} s(p) \\ 0 \end{bmatrix} + \begin{bmatrix} J_p \\ \frac{\sigma_i}{\sigma_x} I \end{bmatrix} u(p) \right\|_{L2}^{2}$$

If we make the assumption that the voxels are independent, which is not strictly true when performing reorientations, the optimization of $E_s(u)$ can be broken up in to individual equations for each point p.

$$(J_p^t J_p + \frac{\sigma_i}{\sigma_x} I) u(p) = - J_p^t (F(p) - M^{\circ} s(p))$$

yielding update step

$$u(p) = - (J_p^t J_p + \frac{\sigma_i}{\sigma_x} I)^{-1} J_p^t (F(p) - M \circ s(p))$$

We use the symmetric $J_p = - \frac{J_p(F) + J_p(M \circ s)}{2}$ computation of the Jacobian, where J_p (F) and J_p (M ∘ s) are the Jacobians of the fixed and deformed moving images at the point p. Each iteration of the diffeomorphic demons method can summarized as follows

1. compute an update step u
2. smooth u with a Gaussian filter
3. s ← s ∘ u
4. Deform the moving image using s
5. Apply reorientation if needed

This process is repeated until the update steps no longer substantially reduce the image difference. The deformation field s is then applied to the moving image resulting in the final deformed subject image.

Appendix B. Spatially Coherent Normalized Cuts

The normalized cuts (N-Cut) algorithm (Shi and Malik 2000; Rahimi and Recht 2004) is a means of partitioning a set of data points x, in our case a set of white matter voxels, based on a provided similarity measure k(x, y). Using the similarity measure we build an affinity matrix such that $K_{i,j} = k(x_i, x_j)$. The affinity matrix describes the weights of a fully connected undirected graph using x as the nodes. The N-cut algorithm labels each node dividing the vertices into 2 sets A and B. The cost Cut(A, B) is the sum of all connections between elements of A and elements of B. The goal is to find the labeling that minimizes the

normalized cut, Cut(A, B)/(Vol(A) + Vol(B)) where Vol() is the sum of the weights within a set.

The labeling is found via a relaxation to the above problem by finding the second largest eigenvector, v, of the matrix $D^{-\frac{1}{2}} K D^{-\frac{1}{2}}$. Where D is a diagonal matrix whose iith element is the sum of all elements in the ith row of K. The labels are determined by examining the sign of v. For a more complete discussion please see (Rahimi and Recht 2004).

Our application of the N-Cut algorithm concerns the ability to label WM voxels based on their FOD. As discussed above we use a product of two Gaussian kernels with standard deviations of σ_f and σ_s as the basis of our similarity measure yielding the following similarity measure:

$$k(x_i, x_j) = e^{\frac{\left\|f_i - f_j\right\|_{L2}^2}{2\sigma_f^2}} e^{\frac{\left\|p_i - p_j\right\|^2}{2\sigma_s^2}}$$

where x_i and x_j are WM voxels with f_i, f_j, p_i, and p_j being the corresponding FODs and spatial locations.

Given a collection of WM voxels we compute the affinity matrix K using the above similarity function. The matrix D is then compute and the second largest eigenvector, v, of $D^{-\frac{1}{2}} K D^{-\frac{1}{2}}$ is determined using the SLEPc (Hernandez, Roman et al. 2005) software package. Two new regions are then determined based on the sign of v.

These two regions are then input into a simple seed growing algorithm (described in Appendix C) which divides them into their spatially disconnected subregions yielding a set of spatially connected regions from the single region with high variance.

Appendix C. Seed Growing Algorithm

A seed growing algorithm is used to divide a supplied region into spatially disconnected subcomponents. This insures that each of the final resulting regions is fully spatially connected. The algorithm is supplied with a list of voxels, X, comprising the region to be divided and returns a list of labels, L, which identify which connected subcomponent each voxel is a member of. The mechanics of the algorithm are shown below:

```
Input: list of voxels, X
Output: list of labels, L
label Value = 1
label Members = Ø
for all x in X do
if x is not labeled then
add x label Members
repeat
y = next element of label Members
L[y] = label Value
Add all unlabeled neighbors to label Members
Until all members of label Members have been visited
label Value = label Value +1
label Members = Ø
```

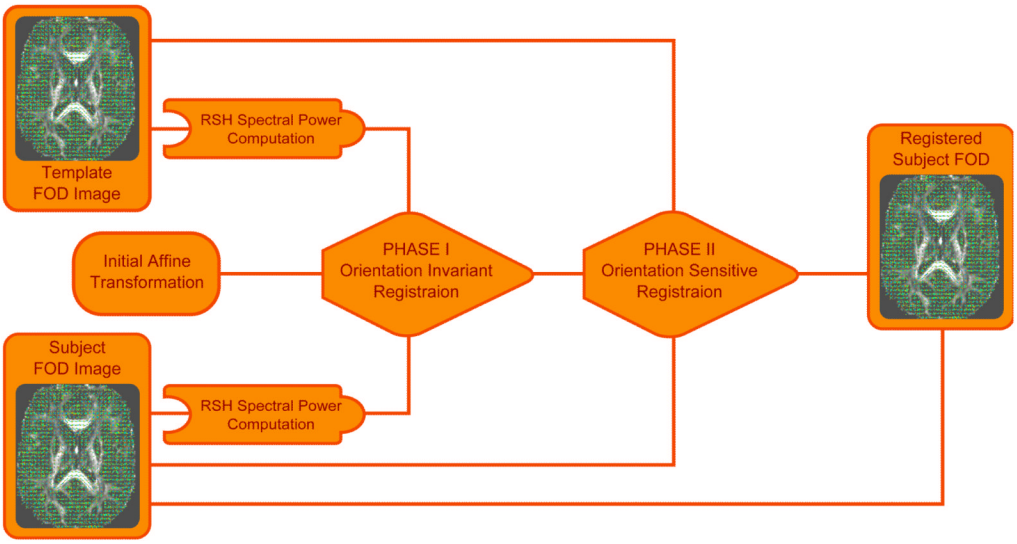

Figure 1.

FOD registration is accomplished using a two phase registration scheme. First spectral power features are computed and registered. This registration is then improved during a second registration phase where the FODs are directly registered while reorienting the FOD at each iteration

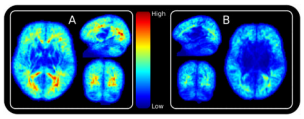

Figure 2.

Effect of Registration on lowering voxelwise population FOD variance. FOD variance maps are shown for affine (A) and non-linear registration (B) methods. The global and focal decrease in population variance clearly demonstrates the importance of using the non-linear registration algorithm for atlas generation.

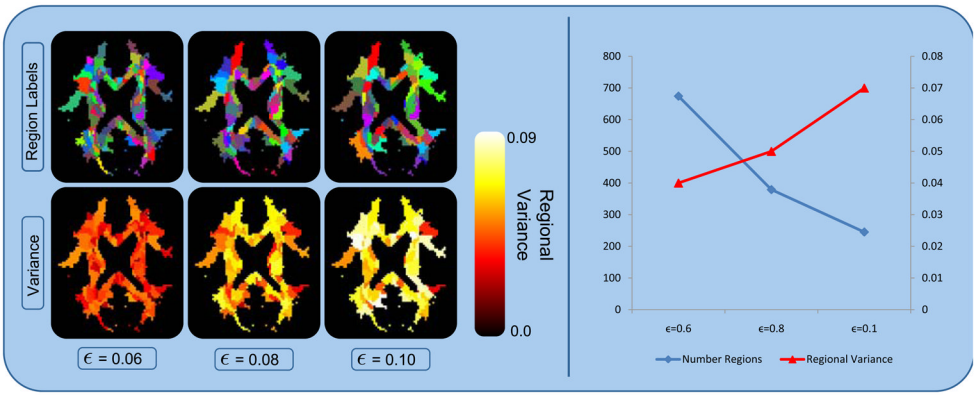

Figure 3.

As the stopping variance threshold, ε is decreased, the expected decrease in the regional FOD variance is seen. This decrease coincides with an increase in the number of regions as well as an increase in the coarseness of the parcellation results.

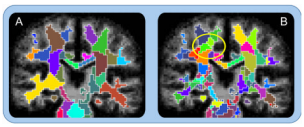

Figure 4.

The general anatomical bilateral symmetry is apparent in the atlas regions. At a higher stopping variance of ε=0.15 (A), this symmetry is more apparent than in the finer regions obtained using a lower stopping variance of ε=0.08 (B) where the division of complex regions is more heavily influence by the local characteristics of the data. For instance the two regions circled in panel B correspond to a single contralateral region.

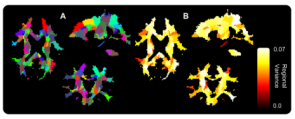

Figure 5.
Population Atlas generated from 23 young adolescents generated using the parameters σ_s =6mm, σ_f = 0.3 and ε = 0.08. Representative slices are shown of the label map indentifing homogenous WM regions (A) and the corresponding FOD variance (B) images.

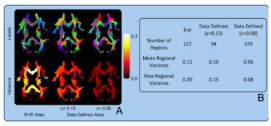

Figure 6.

Representative slices of the EVE-DTI atlas' anatomically defined regions and their corresponding regional FOD variances are shown in panel A, compared with the data defined WM regions generated using two stopping variances ε= 0.15 and 0.08. The EVE-DTI anatomical regions are conspicuously more heterogeneous, indicated by high regional variance, even in central WM areas. A table listing characteristics of each parcellation is shown in panel B.